

2-Methylhexane Cracking on Y Zeolites: Catalytic Cycles and Reaction Selectivity

G. Yaluris,^{*,1} R. J. Madon,^{†,2} and J. A. Dumesic^{*,2}

^{*} Center for Clean Industrial and Treatment Technologies, Department of Chemical Engineering, University of Wisconsin, Madison, Wisconsin 53706;

[†] Engelhard Corporation, 101 Wood Avenue, Iselin, New Jersey 08830

Received May 20, 1996; revised September 13, 1996; accepted September 30, 1996

We have formulated a quantitative kinetic model for analyzing the catalytic cracking of 2-methylhexane over USY-zeolite-based catalysts. The model is based on carbocation chemistry which includes carbenium ion initiation, isomerization, olefin desorption, β -scission, oligomerization, and hydride ion transfer reactions. It describes the complex product distribution at different reaction conditions and for catalysts with different Brønsted acid strengths. Three catalytic cycles dominate this reaction and determine activity and selectivity: the initiation/desorption, initiation/ β -scission, and hydride ion transfer/ β -scission cycles. The rates of these cycles decrease with increasing steaming severity, which reduces catalyst acid strength. The overall site time yield for 2-methylhexane cracking decreases as severity of steaming increases. Because the cycles do not produce excess paraffins, the paraffin to olefin ratio is always lower than 1. β -Scission reactions follow initiation and hydride ion transfer reactions and are important reactions of 2-methylhexane cracking. Olefin adsorption-desorption reactions determine surface coverage of carbenium ions, and although these reactions are in quasi-equilibrium, they play a crucial role in influencing the rates of other surface processes. © 1997 Academic Press

INTRODUCTION

Environmental and constantly changing refinery demands necessitate formulation of fluid catalytic cracking (FCC) catalysts that give product yields tailored to the particular needs of a refiner. To achieve this control one needs to understand the chemistry of catalytic cracking and its dependence on catalyst properties. Because of the complexity of gas oil cracking, most researchers have focused their efforts on studying the cracking chemistry of small hydrocarbon compounds (1–16). These efforts have helped achieve understanding of carbenium ion chemistry over solid acids, and there is now a measure of consensus as to essential aspects of the reaction chemistry in catalytic cracking.

¹ Current address: W. R. Grace & Co., Washington Research Center, 7500 Grace Drive, Columbia, MD 21044.

² To whom correspondence should be addressed.

Efforts have recently been made to model and quantify the reaction chemistry involved in catalytic cracking (17–21). The large number of reactions and products makes it difficult to obtain quantitative relationships between reaction conditions, catalyst properties, catalytic activity, and selectivity. Fundamental models developed by Froment and co-workers for various hydrocarbon reactions (22–27) have effectively predicted product distributions. More recently, Wojciechowski and co-workers (16, 28) estimated reaction path probabilities for 2-methylpentane and 2-methylhexane at initial stages of the cracking reaction.

In our studies, we have quantified the dependence of known surface carbenium ion reaction chemistry on catalyst and reaction parameters. For isobutane (29–32), we showed how the overall cracking process can be described in terms of catalytic cycles that are composed of carbenium ion initiation, β -scission, oligomerization, olefin desorption, isomerization, and hydride ion transfer reactions. These cycles are coupled to one another, and the model predicts their changes with changing conditions. One advantage of this approach is that it provides a comprehensive description of the reaction over a wide range of conversions, not just at very low conversion as in the case of reaction path probability estimation (16). The model gives turnover frequencies of all reactions at any point in the reactor. Finally, since the model includes parameters that represent catalyst properties, we are able to quantify effects of catalyst properties on the chemistry of catalytic cracking.

Recently, we demonstrated the usefulness of this approach for modeling catalytic cracking by successfully extending the model for isobutane cracking to the cracking of 2-methylhexane over commercial USY zeolite-based catalysts (33). However, since the overall cracking scheme for the larger 2-methylhexane has more reaction pathways, the catalytic cycles that dominate the overall reaction are different than those that dominate isobutane cracking.

In this paper, we present a detailed account of our study of 2-methylhexane cracking and describe quantitatively the catalytic cycles that manifest during the cracking process. The paper also addresses the effect of conversion and

Brønsted acid strength on the rates of the catalytic cycles and consequently on reaction selectivity.

EXPERIMENTAL

The USY-based FCC catalyst was made via the Engelhard *in situ* zeolite crystallization process (34–36) in which Y zeolite is crystallized on a calcined kaolin microsphere. The final catalysts, after exchange with ammonium nitrate to remove sodium cations, contained 0.3 wt% Na₂O. The three catalysts discussed in this paper were steamed by fluidizing in 100% steam at atmospheric pressure before use in kinetic measurements. Catalyst USY-S1 was steamed at 1030 K for 2 h, catalyst USY-S2 was steamed for 5 h at 1060 K, and catalyst USY-S3 was steamed for 24 h at 1060 K. Physical properties of these catalysts are listed in Table 1. The surface area of the entire sample minus the surface area of pores larger than 2 nm in diameter, obtained as a “t” plot, gave the microporous surface area. The latter area is mainly that of the zeolite component. Unit cell size measurements via X-ray diffraction were performed using a Si standard, and the framework Al per unit cell was obtained via the correlation given by Sohn *et al.* (37).

We carried out the kinetic experiments in a standard flow unit as described earlier (29, 33). We used Pyrex flow reactors in which the top of the reactor was filled with quartz rings to serve as a preheating zone, while the catalyst was supported in the lower third of the reactor with quartz wool. Catalysts USY-S2 and USY-S3 were studied in a larger reactor due to the larger amount of catalyst needed than USY-S1 to achieve the desired conversions. The size of the reactor influences the amount of products from gas phase thermal reactions, as discussed below. A mixture of 10 mol% 2-methylhexane in He (Liquid Carbonic, 99.999% purity) was used in all experiments, and total flow rates were adjusted to achieve the desired conversion. Reaction products were collected in a multiport Valco valve in separate sampling

loops (20 cm³). The first sample was collected after ~1 min reaction time, and typically four samples were collected at time intervals of 1–2 min. The data reported here are usually from the first loop. No selectivity changes were observed from one loop to the other, while conversions changed only slightly due to catalyst deactivation. The catalyst was purged between runs with flowing He (200 cm³/min) for about 2 h and then regenerated in flowing air (200 cm³/min) at 773 K for 8 h.

We analyzed hydrogen and hydrocarbon products simultaneously with an automated multivalved Hewlett Packard 5890A gas chromatograph containing two columns and two detectors. A 150-m capillary column (Supelco Petrocol DH150) provided complete separation of the hydrocarbon products, and amounts as low as 0.0005 mol% were detected with a flame ionization detector. A Porapak P column was used to separate hydrogen from the hydrocarbons and was detected by a thermal conductivity detector.

We used infrared spectroscopy of adsorbed pyridine to measure Brønsted and Lewis acidity. The experiments were carried out in a diffuse reflectance mode using a Spectra Tech controlled-environment chamber in a Perkin-Elmer 1750 spectrometer. Measurements were quantified using extinction coefficients that were specifically obtained for this instrument using a series of aluminosilicate samples. Experimental details are given elsewhere (38), and the results are presented in Table 1. Finally, we used microcalorimetric measurements of the differential heats of ammonia adsorption at 423 K to probe the acid site strength distributions of the catalysts (30, 39).

MODEL FORMULATION FOR 2-METHYLHEXANE CRACKING

In Refs. (33, 40), we detailed the development and parameterization of a reaction kinetic model for 2-methylhexane cracking. Briefly, the model is defined by a scheme of reactions that describe catalytic cracking of 2-methylhexane and by a thermodynamically consistent set of preexponential factors and activation energies.

Reaction Scheme

Figure 1 shows the reaction scheme used earlier for 2-methylhexane cracking (33). This scheme is based on carbocation chemistry and accounts for all important reaction products. Since kinetic analyses cannot distinguish between different initiation processes (1, 2, 6, 41), we assumed for simplicity that carbenium ions are initiated via protolysis (29). The results of the model suggest that olefin desorption and carbenium ion isomerization are at quasi-equilibrium (29). Since the experimental data indicated that large carbenium ions did not desorb as olefins to a significant degree, we limited desorption of carbenium ions to those with six or fewer carbon atoms.

TABLE 1

Properties of Catalysts USY-S1, USY-S2, and USY-S3

Catalyst	USY-S1	USY-S2	USY-S3
Zeolite surface area (m ² /g)	233	203	178
Total surface area (m ² /g)	371	332	297
Zeolite content ^a (%)	32	28	25
Unit cell size (Å)	24.33	24.27	24.266
Al _F ^b	9.85	3.43	3.00
Si/Al	18.5	55.0	63
Brønsted sites (μmol/g)	129	15.4	6.3
Lewis sites (μmol/g)	164	37.2	27.5
ΔH ₊ (kcal/mol)	166.7	167.6	168.2

^a From BET measurements assuming surface area of pores <2 nm is mainly due to the Y-zeolite.

^b Number of framework Al atoms per unit cell.

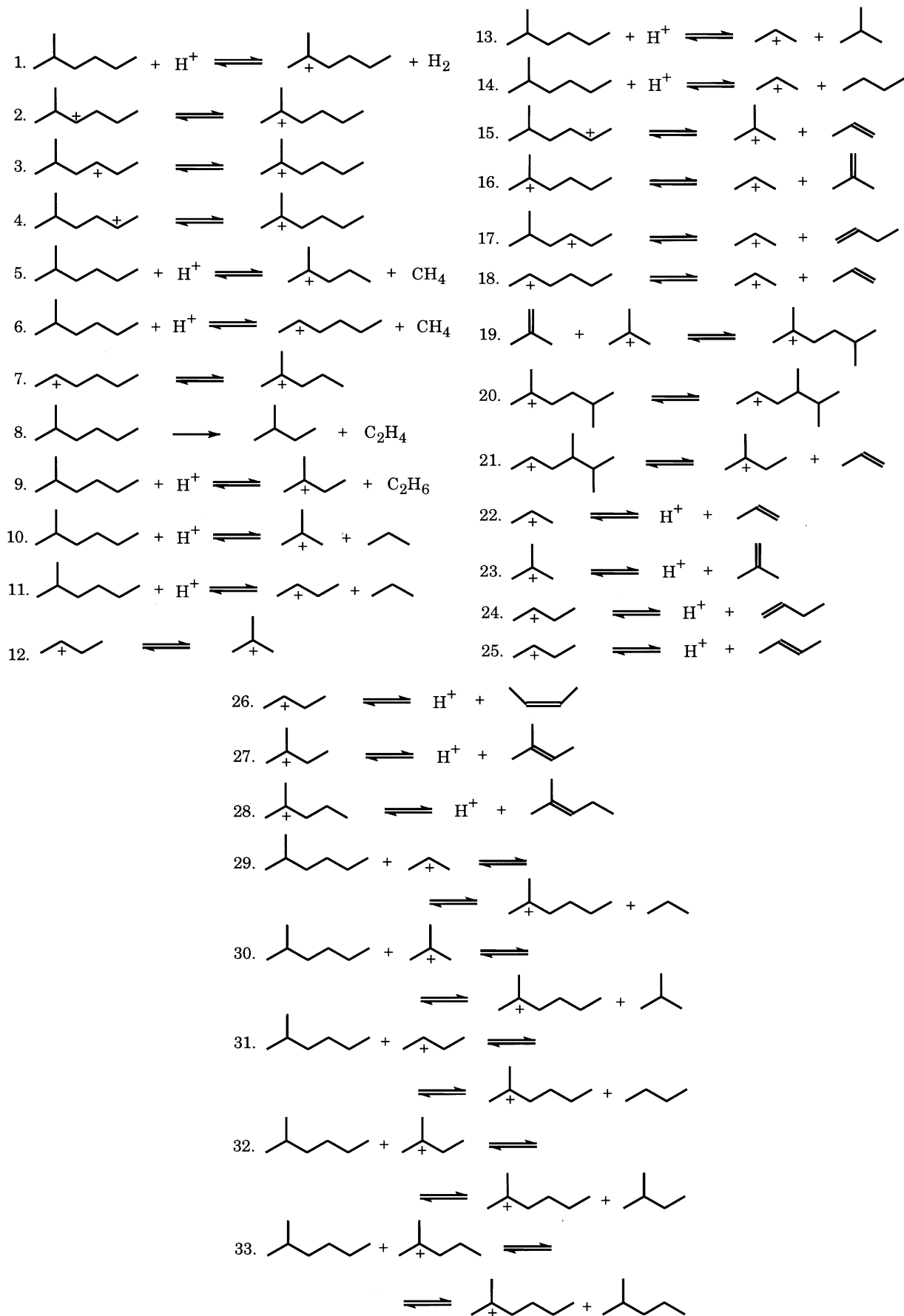


FIG. 1. Reaction scheme for 2-methylhexane cracking.

Although some reports claim to have identified positively charged hydrocarbon intermediates (42), carbenium ions have not been observed by infrared or other spectroscopic techniques on solid acid catalysts during catalytic cracking. The presence of such ions on the catalytic surface has been inferred from product distributions which are consistent with carbenium ion mechanisms observed during cracking reactions in liquid acid systems (43, 44). The ground state of the adsorbed species may be a neutral species, such as an alkoxide species, with the carbenium ion being a short-lived intermediate state in the reaction. In this case, the enthalpy of the reaction from the alkoxide to the carbenium ion state is included in the activation energies we estimate in our model. *Thus, our model involving carbonium ions is kinetically equivalent to a model involving surface alkoxy species, provided that the surface coverages by reactive intermediates are low.*

Recently, Bamwenda *et al.* (16) studied the reactions of 2-methylhexane over a mildly steamed USY zeolite and proposed a reaction mechanism that utilized these same concepts of carbocation chemistry. However, they chose to include in their mechanism a number of disproportionation reactions between surface carbenium ions and gas phase 2-methylhexane. While disproportionation reactions are possible, and we have examined the possibility for methide transfer in the case of isobutane cracking (30), there is no significant evidence to build a reaction scheme on such reactions. Our model predicts the reaction products over a wide range of conversions and catalysts without the need for introducing disproportionation reactions. We will discuss this issue in a later section.

Finally, since the surface concentration of primary carbenium ions on Y zeolites is expected to be negligible, we included ethylene formation from 2-methylhexane as an irreversible, nonelementary step (step 8), probably taking place on electron acceptor sites (29). In the reaction scheme proposed by Bamwenda *et al.* (16), isopentane is allowed to form by the protolytic cracking of 2-methylhexane which leaves primary ethyl cations on the surface. Under the conditions of this study, the two reaction steps are kinetically equivalent.

Parameters

The preexponential factors for the reaction scheme of Fig. 1 were estimated earlier (29, 33, 40) using transition state theory. According to this theory the preexponential factor, A , for a reaction step may be estimated using the simplified equation

$$A = \frac{k_B T}{h} e^{\Delta S^\ddagger/R},$$

where k_B and h are the Boltzmann and Planck constants, respectively, and ΔS^\ddagger is the entropy change from reactants to the transition state. We have previously described the

procedure to estimate entropies of all species included in the reaction scheme of Fig. 1 (29). Importantly, this procedure is used simply to generate a reasonable set of preexponential factors that are consistent with the overall reaction thermodynamics.

We obtained a thermodynamically consistent set of activation energies using the Evans–Polanyi correlation (29, 32),

$$E_\alpha = E_0 + \alpha \Delta H,$$

where ΔH is the heat of reaction, and E_0 and α are constants for a given reaction family, which is defined as a set of reactions with similar reaction chemistry (33). For simplicity, we set α equal to 0.5 for all reactions. Evans–Polanyi constants of reactions at pseudoequilibrium are not kinetically significant, and they were set equal to zero. Since enthalpies of formation of surface species are not available, we used the following adjustable parameter to estimate the heats of reactions from gas phase enthalpy data: ΔH_+ , the heat of stabilization of a carbenium ion relative to the heat of stabilization of a proton at the acid site. In our model, this parameter represents the Brønsted acid strength of the catalyst and relatively small changes in its value represent significant changes in catalyst acid strength.

Our reaction scheme does not directly include gas phase radical cracking. However, we accounted for such cracking by including reaction products obtained in an empty reactor (at the same temperature and flow rate used in the experiments) as part of the feed to the catalyst bed. We assumed that only Brønsted acid sites were active for catalytic cracking (29). Since kinetic parameters of related reactions should remain unchanged for different reactants, we used estimates of Evans–Polanyi parameters from our previous work on isobutane cracking for the same reaction families of 2-methylhexane cracking (33). This procedure decreased the number of adjustable parameters for 2-methylhexane cracking to 12 (ΔH_+ and Evans–Polanyi constants of steps 1, 5, 8, 10, 11, 16, and 29–33). We subsequently used this model to analyze experimental data for 2-methylhexane cracking over USY-S1. A total of 102 independent responses were simulated. Table 2 shows the estimated activation energies.

According to our earlier work (29, 33) the Evans–Polanyi constants of all reactions, except those of initiation steps, do not depend on the catalyst used. This similarity reduces the number of adjustable parameters required for analyzing data collected over USY-S2 and USY-S3. Thus, the 153 independent responses available for USY-S2, and the 119 independent responses available for USY-S3 were analyzed using only five adjustable parameters (ΔH_+ and four Evans–Polanyi constants of initiation steps 1, 5, 8, and 11). To better fit the ratio of isobutane versus *n*-butane formed over USY-S2 and USY-S3, the Evans–Polanyi parameter for step 31 was allowed to change, but it was kept the same

TABLE 2

Reaction Enthalpy Changes and Activation Energies for USY-S1 Estimated at 773 K for Reaction Steps in 2-Methylhexane Cracking

	Catalyst USY-S1, $\Delta H_+ = 166.7 \text{ kcal mol}^{-1}$			
	ΔH_{rxn} (kcal mol ⁻¹)	E_0 (kcal mol ⁻¹)	$E_{\alpha, \text{for}}$ (kcal mol ⁻¹)	$E_{\alpha, \text{rev}}$ (kcal mol ⁻¹)
Step 1	-7.5	37.4	33.6	41.1
Step 2	-18.2	0	0	18.2
Step 3	-18.2	0	0	18.2
Step 4	-18.2	0	0	18.2
Step 5	-22.7	46.3	34.9	57.7
Step 6	-2.7	39.7	38.4	41.1
Step 7	-20.0	0	0	20.0
Step 8	21.6	23.1	33.9	12.3
Step 9	-19.7	46.3	36.5	56.2
Step 10	-17.6	70.0	61.2	78.9
Step 11	0	31.7	31.7	31.7
Step 12	-17.6	0	0	17.6
Step 13	0.03	31.7	31.7	31.7
Step 14	1.92	39.7	40.7	38.8
Step 15	2.52	35.1	36.3	33.8
Step 16	36.8	29.8	48.2	11.4
Step 17	22.5	20.0	31.2	8.77
Step 18	21.1	29.8	40.4	19.3
Step 19	-19.3	35.1	25.4	44.7
Step 20	18.0	0	18.0	0
Step 21	3.38	18.7	20.4	17.1
Step 22	18.4	0	18.4	0
Step 23	34.5	0	34.5	0
Step 24	20.8	0	20.8	0
Step 25	18.0	0	18.0	0
Step 26	18.4	0	18.4	0
Step 27	34.4	0	34.4	0
Step 28	36.1	0	36.1	0
Step 29	-19.9	22.5	12.6	32.5
Step 30	-2.28	25.2	24.1	26.3
Step 31	-18.0	20.4	11.4	29.4
Step 32	-0.47	26.2	26.0	26.4
Step 33	0.75	22.5	22.9	22.2

for both catalysts. Table 3 shows the estimated activation energies for USY-S3.

RESULTS

Product Distributions

The kinetic model predicts the trends in complex product distributions over different catalysts using a limited number of kinetic parameters that are related to the fundamental surface chemistry of carbenium and carbonium ions. Tables 4 and 5 show excellent concurrence between experimental data and model predictions for 2-methylhexane cracking over catalysts USY-S1 and USY-S3, respectively. Figures 2 and 3 show that the trends of site time yields (molecules produced per second per site in the reactor) of paraffins and olefins observed experimentally over USY-S1 and USY-S3 are predicted well by the model.

Figure 4 shows that the model predicts changes in the experimental paraffin to olefin ratios with conversion and catalyst steaming. The ratio increases only slightly with conversion for USY-S1, while it increases to a greater extent for USY-S2 and USY-S3. Regardless of conversion and steaming, the experimental data and the model predictions for the three catalysts indicate that the paraffin to olefin ratio is never greater than 1. In agreement with the results of others (45–49), steaming, which increases the framework Si/Al ratio, results in a decrease of the paraffin to olefin ratio.

Figure 5 shows the distribution of C₃, C₄, C₅, and C₆ species with conversion for USY-S1. The fraction of C₃ species in the C₃–C₆ product stream is near 50%. About 47% of this stream is C₄ species and the balance is C₅ and C₆ species. This composition does not change significantly with conversion or with severity of catalyst steaming.

TABLE 3

Reaction Enthalpy Changes and Activation Energies for USY-S3 Estimated at 773 K for Reaction Steps in 2-Methylhexane Cracking

	Catalyst USY-S3, $\Delta H_+ = 168.2 \text{ kcal mol}^{-1}$			
	ΔH_{rxn} (kcal mol ⁻¹)	E_0 (kcal mol ⁻¹)	$E_{\alpha, \text{for}}$ (kcal mol ⁻¹)	$E_{\alpha, \text{rev}}$ (kcal mol ⁻¹)
Step 1	-5.95	35.3	32.3	38.3
Step 2	-18.2	0	0	18.2
Step 3	-18.2	0	0	18.2
Step 4	-18.2	0	0	18.2
Step 5	-21.2	46.4	35.8	57.0
Step 6	-1.17	39.7	39.2	40.3
Step 7	-20.0	0	0	20.0
Step 8	21.6	25.0	35.8	14.2
Step 9	-18.2	46.4	37.3	55.5
Step 10	-16.1	70.0	62.0	78.0
Step 11	1.54	34.8	35.6	34.0
Step 12	-17.6	0	0	17.6
Step 13	1.57	34.8	35.6	34.0
Step 14	3.47	39.7	41.5	38.0
Step 15	2.52	35.1	36.3	33.8
Step 16	36.8	29.8	48.2	11.4
Step 17	22.5	20.0	31.2	8.77
Step 18	21.1	29.8	40.4	19.3
Step 19	-19.3	35.1	25.4	44.7
Step 20	18.0	0	18.0	0
Step 21	3.38	18.7	20.4	17.1
Step 22	16.9	0	16.9	0
Step 23	33.0	0	33.0	0
Step 24	19.2	0	19.2	0
Step 25	16.5	0	16.5	0
Step 26	16.9	0	16.9	0
Step 27	32.8	0	32.8	0
Step 28	34.6	0	34.6	0
Step 29	-19.9	22.5	12.6	32.5
Step 30	-2.28	25.2	24.1	26.3
Step 31	-18.0	21.5	12.5	30.5
Step 32	-0.47	26.2	26.0	26.4
Step 33	0.75	22.5	22.9	22.2

TABLE 4

Experimental Data and Model Predictions for 2-Methylhexane Cracking over USY-S1 at 773 K and at Different Space Velocities

S_V^{-1} (g h mol ⁻¹)	4.04		6.48		8.28		8.08		10.26		11.11	
Pressure (kPa)	129.8		125		123.4		121.7		120.9		119.4	
Conversion (%)	9.2		15.4		18.9		20.5		24.6		28.4	
	Exp	Model	Exp	Model	Exp	Model	Exp	Model	Exp	Model	Exp	Model
Hydrogen	0.055	0.060	0.088	0.083	0.065	0.100	0.110	0.099	0.118	0.116	0.132	0.115
Methane	0.052	0.044	0.063	0.060	0.075	0.074	0.064	0.078	0.086	0.086	0.075	0.092
Ethylene	0.061	0.056	0.082	0.080	0.095	0.100	0.077	0.101	0.116	0.116	0.098	0.119
Ethane	0.013	0.011	0.016	0.015	0.018	0.019	0.019	0.019	0.021	0.022	0.022	0.023
Propylene	0.686	0.543	1.095	0.985	1.341	1.428	1.525	1.353	1.717	1.868	2.024	1.918
Propane	0.157	0.195	0.311	0.319	0.397	0.433	0.408	0.412	0.551	0.548	0.591	0.548
Isobutane	0.437	0.400	0.790	0.741	0.995	1.085	1.061	1.023	1.338	1.427	1.484	1.468
<i>n</i> -Butane	0.070	0.050	0.124	0.104	0.152	0.163	0.167	0.153	0.206	0.223	0.229	0.232
C ₄ olefins	0.280	0.271	0.412	0.424	0.495	0.557	0.584	0.538	0.616	0.685	0.748	0.686
2-Methyl-2-butene	0.006	0.006	0.013	0.011	0.015	0.017	0.017	0.016	0.021	0.023	0.027	0.024
Isopentane	0.027	0.040	0.061	0.062	0.079	0.080	0.070	0.076	0.111	0.098	0.111	0.095
Isohexane	0.012	0.013	0.022	0.020	0.026	0.027	0.025	0.025	0.033	0.033	0.035	0.033

Note. All values are mol% of the reactor effluent stream.

Finally, we list turnover frequencies (TOF, molecules consumed or produced per site per second at a specific point in the reactor) for all reaction steps of the model in Tables 6 and 7. Table 6 lists the rates of 2-methylhexane reactions over USY-S1 at the reactor entrance and exit at 773 K and 15% conversion. Table 7 compares rates on USY-S1 at 15 and 28% conversion, and USY-S2 and USY-S3 at 773 K and ca. 15% conversion.

Effects of Catalyst Steaming

Figure 6 shows the differential heats of ammonia adsorption versus adsorbate coverage on USY-S1, USY-S2, and USY-S3 at 423 K. Figure 7 shows histograms of acid site

strength distributions for the same catalysts. We obtained these histograms by first fitting the differential heats of adsorption data with a polynomial and then using it to estimate the amount of adsorbed ammonia within a range of differential heats. The data in these figures show that both the number of acid sites and the acid strength decrease as the severity of the steaming increases from USY-S1 to USY-S3. About 16% of the acid sites on USY-S1 have a heat of ammonia adsorption around 120 kJ/mol. However, when the catalyst is steamed further, almost all of these sites are eliminated. These strong sites are replaced on USY-S2 and USY-S3 by sites that adsorb ammonia with differential heats near 110 kJ/mol and lower. Although differences in the acid site strength distributions of USY-S2 and USY-S3

TABLE 5

Experimental Data and Model Predictions for 2-Methylhexane Cracking over USY-S3 at 773 K and at Different Space Velocities

S_V^{-1} (g h mol ⁻¹)	91.7		125		204.1		263.2		303		370.4		555.6	
Pressure (kPa)	140.8		133		126.3		122.1		122.8		121.3		120.9	
Conversion (%)	4.4		6.0		10.4		14.3		14.9		20.4		32.2	
	Exp	Model	Exp	Model	Exp	Model	Exp	Model	Exp	Model	Exp	Model	Exp	Model
Hydrogen	0.118	0.148	0.158	0.188	0.276	0.274	0.410	0.326	0.385	0.378	0.549	0.429	0.769	0.592
Methane	0.047	0.051	0.063	0.070	0.103	0.100	0.116	0.114	0.138	0.124	0.161	0.134	0.194	0.151
Ethylene	0.043	0.043	0.054	0.059	0.077	0.084	0.085	0.096	0.102	0.105	0.118	0.114	0.141	0.131
Ethane	0.010	0.011	0.015	0.016	0.020	0.022	0.024	0.026	0.029	0.028	0.033	0.031	0.043	0.037
Propylene	0.357	0.296	0.491	0.424	0.835	0.739	1.146	0.956	1.194	1.200	1.612	1.483	2.513	2.568
Propane	0.023	0.029	0.035	0.042	0.070	0.078	0.109	0.105	0.120	0.137	0.170	0.178	0.386	0.353
Isobutane	0.141	0.113	0.206	0.180	0.394	0.365	0.573	0.501	0.616	0.662	0.881	0.859	1.530	1.647
<i>n</i> -Butane	0.012	0.010	0.018	0.016	0.034	0.034	0.051	0.046	0.055	0.062	0.078	0.081	0.157	0.156
C ₄ olefins	0.210	0.198	0.275	0.264	0.437	0.400	0.571	0.484	0.582	0.569	0.747	0.659	1.065	0.975
2-Methyl-2-butene	0.002	0.005	0.005	0.006	0.008	0.010	0.011	0.014	0.011	0.018	0.017	0.022	0.032	0.042
Isopentane	0.012	0.014	0.016	0.019	0.026	0.029	0.035	0.036	0.038	0.044	0.055	0.053	0.094	0.086
Isohexane	0.009	0.009	0.011	0.012	0.018	0.018	0.022	0.021	0.023	0.026	0.034	0.030	0.045	0.051

Note. All values are mol% of the reactor effluent stream.

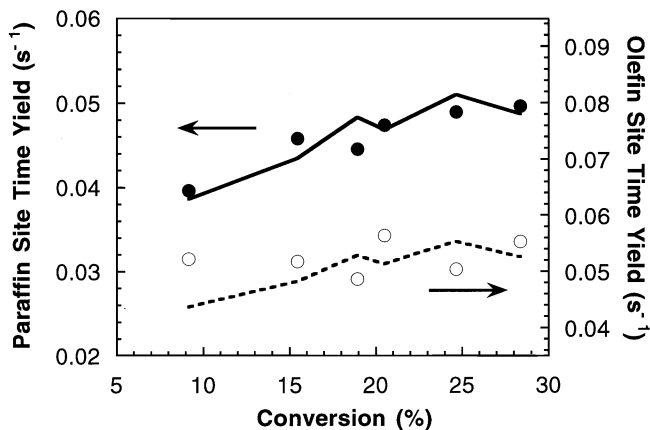


FIG. 2. Simulated and experimental paraffin and olefin site time yields for 2-methylhexane cracking over USY-S1 at 773 K and various conversions. Points represent experimental data.

are small, USY-S2 appears to be a slightly stronger solid acid than USY-S3. Such changes in acidity due to steaming have been previously discussed by us (30) and by Chen *et al.* (38).

The model predicts that increasing steam treatment severity increases the value of ΔH_+ , the heat of stabilization of a carbenium ion on the catalytic surface with respect to the heat of stabilization of a proton, which represents the Brønsted acid strength of the catalyst. The value of ΔH_+ changes by 0.9 kcal/mol from USY-S1 to USY-S2 and 0.6 kcal/mol from USY-S2 to USY-S3, indicating that the stability of carbenium ions on the surface and therefore the catalyst acid strength decreases from USY-S1 to USY-S3. The confidence limits of the values of ΔH_+ reported in Table 1 are ± 0.3 kcal/mol. In agreement with the microcalorimetric data, the model results suggest that the acid strength difference between USY-S1 and USY-S2 is larger than that between USY-S2 and USY-S3.

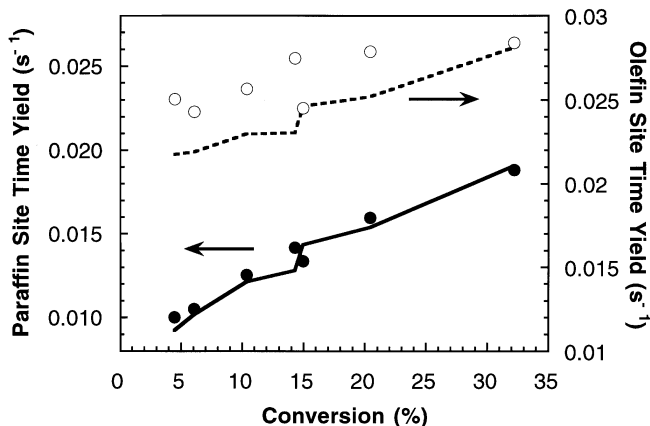


FIG. 3. Simulated and experimental paraffin and olefin site time yields for 2-methylhexane cracking over USY-S3 at 773 K and various conversions. Points represent experimental data.

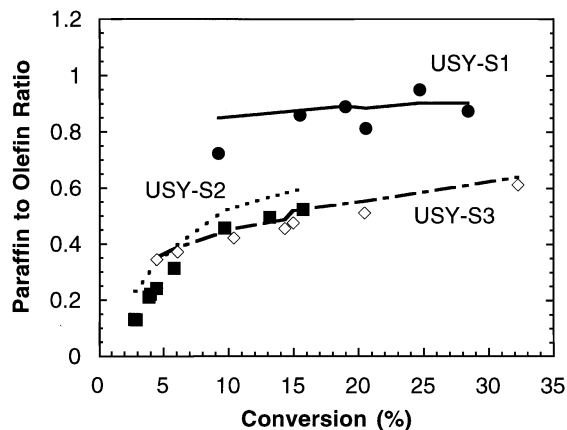


FIG. 4. Simulated and experimental paraffin to olefin ratios for 2-methylhexane cracking over USY-S1, USY-S2, and USY-S3 at 773 K and various conversions. Paraffins and olefins with more than three carbon atoms are counted. Points represent experimental data.

The reduction in catalyst acid strength caused by steaming is accompanied by a decrease in the activity of the average catalytic site. At a conversion of ca. 15%, the site time yield for 2-methylhexane conversion is $5 \times 10^{-2} \text{ s}^{-1}$ for catalyst USY-S1, $2.7 \times 10^{-2} \text{ s}^{-1}$ for catalyst USY-S2, and $2 \times 10^{-2} \text{ s}^{-1}$ for catalyst USY-S3. These kinetic measurements are in agreement with microcalorimetric data and model predictions that increasing severity of steam treatment of FCC catalysts decreases their Brønsted acid strength. The largest change in activity is from USY-S1 to USY-S2, the two catalysts with the largest difference in acid site strength distribution. USY-S2 and USY-S3 with small differences in their acid site strength distributions exhibit only a small difference in catalytic activity per site. In

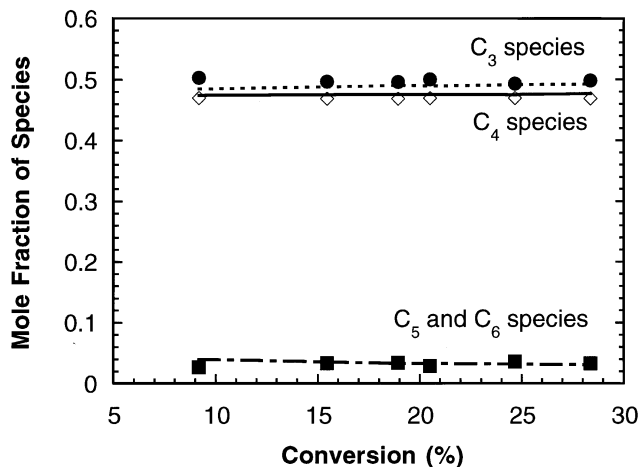


FIG. 5. Simulated and experimental distributions of C_3 (●), C_4 (◇), and C_5 and C_6 (■) species for 2-methylhexane cracking over USY-S1 at 773 K and various conversions. Values in mole fractions of the total amount of C_3 , C_4 , C_5 , and C_6 species in the gas phase. Points represent experimental data.

TABLE 6

Turnover Frequencies of Individual Reaction Steps for 2-Methylhexane Cracking on USY-S1 at 773 K (15.4% Conversion) at Reactor Inlet and Outlet

	Catalyst USY-S1, 15% conversion			
	Reactor entrance (conversion 0.5%)		Reactor outlet (conversion 15%)	
	Forward rate (s ⁻¹)	Net rate (s ⁻¹)	Forward rate (s ⁻¹)	Net rate (s ⁻¹)
Step 1	2.4 × 10 ⁻³	2.4 × 10 ⁻³	2.0 × 10 ⁻³	2.0 × 10 ⁻³
Step 2	7.7 × 10 ²	0	5.0 × 10 ³	0
Step 3	7.7 × 10 ²	-1.2 × 10 ⁻³	5.0 × 10 ³	-6.3 × 10 ⁻³
Step 4	7.7 × 10 ²	-4.5 × 10 ⁻⁵	5.0 × 10 ³	-2.5 × 10 ⁻⁴
Step 5	1.0 × 10 ⁻³	1.0 × 10 ⁻³	8.3 × 10 ⁻⁴	8.3 × 10 ⁻⁴
Step 6	1.1 × 10 ⁻⁴	1.1 × 10 ⁻⁴	8.9 × 10 ⁻⁵	8.9 × 10 ⁻⁵
Step 7	4.6 × 10 ⁴	-2.1 × 10 ⁻⁴	6.3 × 10 ⁴	-4.2 × 10 ⁻⁵
Step 8	2.0 × 10 ⁻³	2.0 × 10 ⁻³	1.7 × 10 ⁻³	1.7 × 10 ⁻³
Step 9	3.8 × 10 ⁻⁴	3.8 × 10 ⁻⁴	3.1 × 10 ⁻⁴	3.1 × 10 ⁻⁴
Step 10	3.9 × 10 ⁻¹¹	3.9 × 10 ⁻¹¹	3.2 × 10 ⁻¹¹	3.2 × 10 ⁻¹¹
Step 11	8.7 × 10 ⁻³	8.7 × 10 ⁻³	7.0 × 10 ⁻³	7.0 × 10 ⁻³
Step 12	1.6 × 10 ⁶	1.5 × 10 ⁻³	1.4 × 10 ⁷	-8.8 × 10 ⁻⁴
Step 13	8.6 × 10 ⁻³	8.6 × 10 ⁻³	7.0 × 10 ⁻³	7.0 × 10 ⁻³
Step 14	2.4 × 10 ⁻⁵	2.4 × 10 ⁻⁵	2.0 × 10 ⁻⁵	2.0 × 10 ⁻⁵
Step 15	4.1 × 10 ⁻⁵	4.1 × 10 ⁻⁵	2.7 × 10 ⁻⁴	2.1 × 10 ⁻⁴
Step 16	7.4 × 10 ⁻³	7.3 × 10 ⁻³	4.8 × 10 ⁻²	3.9 × 10 ⁻²
Step 17	1.1 × 10 ⁻³	1.1 × 10 ⁻³	7.4 × 10 ⁻³	5.9 × 10 ⁻³
Step 18	3.2 × 10 ⁻⁴	3.2 × 10 ⁻⁴	4.4 × 10 ⁻⁴	1.8 × 10 ⁻⁴
Step 19	1.3 × 10 ⁻⁵	1.2 × 10 ⁻⁵	9.2 × 10 ⁻⁴	6.4 × 10 ⁻⁴
Step 20	1.6 × 10 ⁻²	1.2 × 10 ⁻⁵	5.0	6.4 × 10 ⁻⁴
Step 21	4.5 × 10 ⁻⁵	1.2 × 10 ⁻⁵	1.4 × 10 ⁻²	6.4 × 10 ⁻⁴
Step 22	8.0 × 10 ⁵	1.7 × 10 ⁻²	1.6 × 10 ⁶	4.6 × 10 ⁻²
Step 23	2.2 × 10 ⁴	-2.7 × 10 ⁻³	1.8 × 10 ⁵	-3.1 × 10 ⁻²
Step 24	4.7 × 10 ³	5.2 × 10 ⁻⁴	3.9 × 10 ⁴	-4.3 × 10 ⁻³
Step 25	2.7 × 10 ⁴	3.5 × 10 ⁻³	2.3 × 10 ⁵	3.7 × 10 ⁻³
Step 26	2.1 × 10 ⁴	2.3 × 10 ⁻³	1.8 × 10 ⁵	2.5 × 10 ⁻³
Step 27	1.9 × 10 ³	3.7 × 10 ⁻⁴	3.5 × 10 ⁴	6.4 × 10 ⁻⁴
Step 28	1.8 × 10 ³	2.0 × 10 ⁻⁴	2.5 × 10 ³	2.8 × 10 ⁻⁵
Step 29	3.3 × 10 ⁻⁴	3.3 × 10 ⁻⁴	5.8 × 10 ⁻³	5.8 × 10 ⁻³
Step 30	4.2 × 10 ⁻³	4.2 × 10 ⁻³	3.0 × 10 ⁻²	3.0 × 10 ⁻²
Step 31	8.6 × 10 ⁻⁴	8.6 × 10 ⁻⁴	6.1 × 10 ⁻³	6.1 × 10 ⁻³
Step 32	2.5 × 10 ⁻⁵	2.5 × 10 ⁻⁵	4.1 × 10 ⁻⁴	4.1 × 10 ⁻⁴
Step 33	6.1 × 10 ⁻⁴	6.1 × 10 ⁻⁴	7.2 × 10 ⁻⁴	7.2 × 10 ⁻⁴

agreement with our results, Shertukde *et al.* (50) suggest that crowding of extraframework aluminum formed by steaming in zeolite pores, may result in reduced catalytic activity.

A correlation also exists between Brønsted acid strength and catalyst selectivity. At about 15% conversion, the paraffin to olefin ratio decreases from 0.86 for USY-S1 to 0.53 for USY-S2 to 0.48 for USY-S3 (Fig. 4). The most strongly acidic catalyst is the most selective for paraffin formation, and the largest change in selectivity is between catalysts with the largest difference in acid strengths.

Fractional Surface Coverages

The primary attribute of the kinetic model is extraction of reaction rates for specific catalytic cycles. Due to a lack

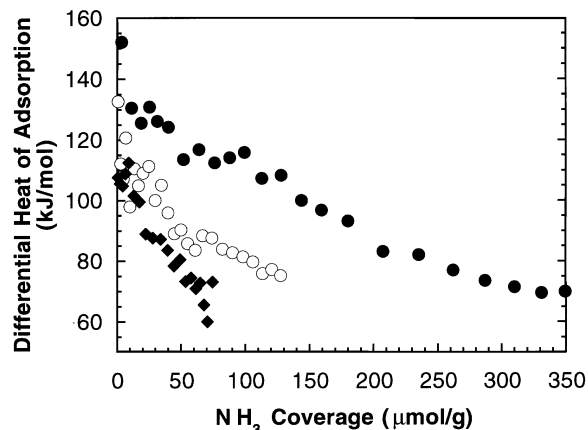


FIG. 6. Differential heats of ammonia adsorption on USY-S1 (●), USY-S2 (○), and USY-S3 (◆) at 423 K.

of information necessary for a more comprehensive model, carbenium ion surface coverages and rate constants can not be estimated independently. Thus, coverages that are different from those estimated here may be obtained if rate constants are adjusted appropriately to compensate. Therefore, for the thermodynamically consistent set of rate constants we have employed, the surface coverages we estimate

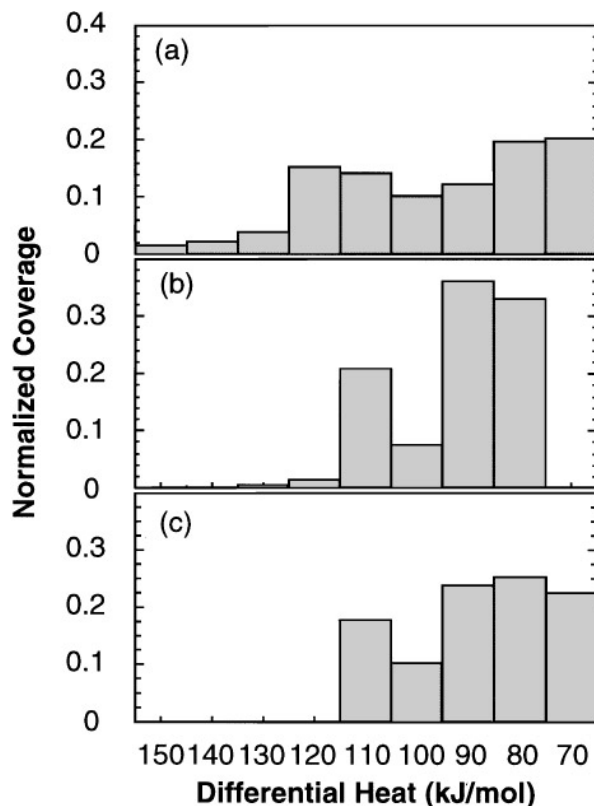


FIG. 7. Acid site strength distributions from NH₃ microcalorimetry at 423 K for (a) USY-S1, (b) USY-S2, and (c) USY-S3. Coverage normalized with respect to the total number of acid sites for each catalyst.

TABLE 7

Turnover Frequencies of Individual Reaction Steps for 2-Methylhexane Cracking on USY-S1 (Conversion 15.4 and 28.4%), USY-S2 (Conversion 15.7%), and USY-S3 (Conversion 14.9%) at Reactor Outlet and 773 K

Catalyst Pressure (kPa) Conversion (%)	USY-S1 125 15.4		USY-S1 119.4 28.4		USY-S2 131.2 15.7		USY-S3 122.8 14.9	
	Forward rate	Net rate	Forward rate	Net rate	Forward rate	Net rate	Forward rate	Net rate
Step 1	2.0×10^{-3}	2.0×10^{-3}	1.4×10^{-3}	1.4×10^{-3}	4.4×10^{-3}	4.4×10^{-3}	4.5×10^{-3}	4.5×10^{-3}
Step 2	5.0×10^3	0	8.1×10^3	0	3.9×10^3	0	2.8×10^3	0
Step 3	5.0×10^3	-6.3×10^{-3}	8.1×10^3	-7.9×10^{-3}	3.9×10^3	-4.6×10^{-3}	2.8×10^3	-3.2×10^{-3}
Step 4	5.0×10^3	-2.5×10^{-4}	8.1×10^3	-3.2×10^{-4}	3.9×10^3	-1.7×10^{-4}	2.8×10^3	-1.2×10^{-4}
Step 5	8.3×10^{-4}	8.3×10^{-4}	6.1×10^{-4}	6.1×10^{-4}	7.9×10^{-4}	7.9×10^{-4}	4.6×10^{-4}	4.6×10^{-4}
Step 6	8.9×10^{-5}	8.9×10^{-5}	6.4×10^{-5}	6.4×10^{-5}	7.1×10^{-5}	7.1×10^{-5}	5.2×10^{-5}	5.2×10^{-5}
Step 7	6.0×10^4	-4.2×10^{-5}	9.4×10^4	4.1×10^{-4}	5.6×10^4	-7.2×10^{-5}	3.6×10^4	-4.0×10^{-5}
Step 8	1.7×10^{-3}	1.7×10^{-3}	1.3×10^{-3}	1.3×10^{-3}	6.4×10^{-4}	6.4×10^{-4}	4.9×10^{-4}	4.9×10^{-4}
Step 9	3.1×10^{-4}	3.1×10^{-4}	2.2×10^{-4}	2.2×10^{-4}	2.9×10^{-4}	2.9×10^{-4}	1.7×10^{-4}	1.7×10^{-4}
Step 10	3×10^{-11}	3×10^{-11}	2×10^{-11}	2×10^{-11}	3×10^{-11}	3×10^{-11}	2×10^{-11}	2×10^{-11}
Step 11	7.0×10^{-3}	7.0×10^{-3}	5.1×10^{-3}	5.1×10^{-3}	4.3×10^{-4}	4.3×10^{-4}	5.4×10^{-4}	5.4×10^{-4}
Step 12	1.4×10^7	-8.8×10^{-4}	2.1×10^7	-2.2×10^{-3}	9.4×10^6	-2.2×10^{-3}	6.9×10^6	-1.8×10^{-3}
Step 13	7.0×10^{-3}	7.0×10^{-3}	5.1×10^{-3}	5.1×10^{-3}	4.3×10^{-4}	4.3×10^{-4}	5.4×10^{-4}	5.4×10^{-4}
Step 14	2.0×10^{-5}	2.0×10^{-5}	1.4×10^{-5}	1.4×10^{-5}	1.6×10^{-5}	1.6×10^{-5}	1.1×10^{-5}	1.1×10^{-5}
Step 15	2.7×10^{-4}	2.1×10^{-4}	4.1×10^{-4}	2.6×10^{-4}	2.1×10^{-4}	1.6×10^{-4}	1.5×10^{-4}	1.1×10^{-4}
Step 16	4.8×10^{-2}	3.9×10^{-2}	7.5×10^{-2}	4.7×10^{-2}	3.7×10^{-2}	2.9×10^{-2}	2.6×10^{-2}	2.0×10^{-2}
Step 17	7.4×10^{-3}	5.9×10^{-3}	1.1×10^{-2}	7.2×10^{-3}	5.7×10^{-3}	4.4×10^{-3}	4.0×10^{-3}	3.1×10^{-3}
Step 18	4.4×10^{-4}	1.8×10^{-4}	6.2×10^{-4}	-2.5×10^{-4}	4.0×10^{-4}	1.6×10^{-4}	2.4×10^{-4}	1.0×10^{-4}
Step 19	9.2×10^{-4}	6.4×10^{-4}	2.2×10^{-3}	1.2×10^{-3}	7.7×10^{-4}	4.6×10^{-4}	6.1×10^{-4}	4.2×10^{-4}
Step 20	5.0	6.4×10^{-4}	1.8×10^1	1.2×10^{-3}	5.4	4.6×10^{-4}	3.5	4.2×10^{-4}
Step 21	1.4×10^{-2}	6.4×10^{-4}	5.0×10^{-2}	1.2×10^{-3}	1.5×10^{-2}	4.6×10^{-4}	9.8×10^{-3}	4.2×10^{-4}
Step 22	1.6×10^6	4.6×10^{-2}	2.9×10^6	5.1×10^{-2}	2.0×10^6	3.0×10^{-2}	2.0×10^6	2.2×10^{-2}
Step 23	1.8×10^5	-3.1×10^{-2}	2.7×10^5	-4.0×10^{-2}	2.3×10^5	-2.0×10^{-2}	2.5×10^5	-2.0×10^{-2}
Step 24	3.9×10^4	-4.3×10^{-3}	5.7×10^4	-6.0×10^{-3}	4.8×10^4	-3.3×10^{-3}	5.3×10^4	-2.2×10^{-3}
Step 25	2.3×10^5	3.7×10^{-3}	3.4×10^5	3.6×10^{-3}	2.8×10^5	2.3×10^{-3}	3.1×10^5	1.8×10^{-3}
Step 26	1.8×10^5	2.5×10^{-3}	2.6×10^5	2.4×10^{-3}	2.2×10^5	1.6×10^{-3}	2.4×10^5	1.2×10^{-3}
Step 27	3.5×10^4	6.4×10^{-4}	6.7×10^4	9.0×10^{-4}	5.5×10^4	4.3×10^{-4}	5.5×10^4	3.8×10^{-4}
Step 28	2.5×10^3	2.8×10^{-5}	3.7×10^3	6.7×10^{-5}	4.0×10^3	2.0×10^{-5}	3.9×10^3	1.4×10^{-5}
Step 29	5.8×10^{-3}	5.8×10^{-3}	8.3×10^{-3}	8.3×10^{-3}	4.3×10^{-3}	4.3×10^{-3}	2.5×10^{-3}	2.5×10^{-3}
Step 30	3.0×10^{-2}	3.0×10^{-2}	3.6×10^{-2}	3.6×10^{-2}	2.2×10^{-2}	2.2×10^{-2}	1.5×10^{-2}	1.5×10^{-2}
Step 31	6.1×10^{-3}	6.1×10^{-3}	7.3×10^{-3}	7.3×10^{-3}	2.1×10^{-3}	2.1×10^{-3}	1.4×10^{-3}	1.4×10^{-3}
Step 32	4.1×10^{-4}	4.1×10^{-4}	6.3×10^{-4}	6.3×10^{-4}	3.7×10^{-4}	3.7×10^{-4}	2.3×10^{-4}	2.3×10^{-4}
Step 33	7.2×10^{-4}	7.2×10^{-4}	8.7×10^{-4}	8.6×10^{-4}	6.8×10^{-4}	6.8×10^{-4}	4.0×10^{-4}	4.0×10^{-4}

should be used for comparative purposes only. The absolute values we report are not necessarily representative of the actual carbenium ion surface coverages (29); however, the trends are important and relevant.

Carbenium ions on the surface are mostly isobutyl cations, although significant amounts of the relatively stable tertiary isopentyl and isohexyl carbenium ions are also predicted to be on the surface. With the exception of the isopentyl and C_8^+ carbenium ions, the coverage by the other carbenium ions is finite at zero conversion. Gas phase olefins are at pseudoequilibrium with surface carbenium ions, and C_3 and C_4 olefins, formed by thermal cracking, can adsorb on the surface and be protonated to yield C_3^+ and C_4^+ carbenium ions. These carbenium ions then react with the same gas phase olefins according to the reaction scheme of Fig. 1 to form C_6^+ and C_7^+ carbenium ions before the catalytic conversion of 2-methylhexane begins.

Figure 8 shows changes in the coverages of propyl, isobutyl, and isohexyl carbenium ions with reactor length (or conversion) for USY-S1. The coverage of C_4^+ , C_5^+ , and C_7^+ carbenium ions increases with increasing conversion, similar to the coverage by isobutyl carbenium ions shown in Fig. 8. The surface coverages of these species depend on the combined rates of initiation and hydride ion transfer processes that produce and consume them. The coverage of propyl cations increases faster at higher conversions because the rate of propylene production increases rapidly with conversion.

The initial increase of the coverage by C_6^+ carbenium ions is due to initiation reactions that produce methane. At higher conversion, β -scission and hydride ion transfer reactions consume these species and the coverage reaches a plateau. As conversion increases further and the concentration of propylene in the gas phase product increases,

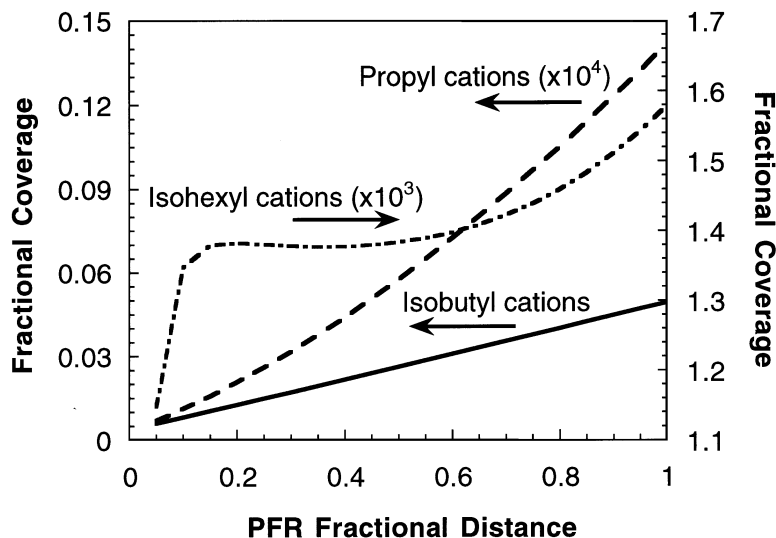


FIG. 8. Surface coverages of propyl (---), isobutyl (—), and isohexyl (- · -) carbenium ions versus reactor length for catalyst USY-S1 at 773 K and 15% conversion.

the reverse rate of step 18 increases (Table 7). Thus, the coverage of C_6^+ species on the catalyst increases with conversion.

Table 8 shows fractional surface coverages of the most abundant surface species predicted by the model for catalysts USY-S1, USY-S2, and USY-S3. The reduction in the acid strength of the catalysts, caused by steaming, decreases the fractional coverages of the surface carbenium ions. Most of the observed reduction of carbenium ion coverage is from USY-S1 to USY-S2, the two catalysts with the largest difference in acid strength. For USY-S2 and USY-S3, the difference in total carbenium ion coverage is smaller.

DISCUSSION

The catalytic cycles involved in hydrocarbon cracking (30, 33) do not change from one catalyst to another, but

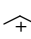
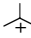
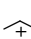
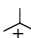
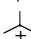
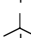
their relative rates may change significantly, thus affecting activity and selectivity. Also, the importance of certain reaction pathways may vary for different hydrocarbon reactants, thus altering the reaction routes via which products are formed. For example, when isobutane is replaced by 2-methylhexane, β -scission reactions become much more important in the cracking of the larger hydrocarbon. Therefore, though the carbenium ion reaction chemistry remains unchanged (33), different cycles dominate the overall reaction.

Figure 9a is a schematic diagram of the catalytic cycles that operate during the cracking of 2-methylhexane at 773 K and ca. 15% conversion over USY-S1 at the reactor outlet. The same cycles take place over USY-S2 and USY-S3. In Fig. 9a, we have grouped several surface and gas phase species together for simplicity, and some cycles presented here are, therefore, a combination of several cycles of similar chemistry. The nomenclature in Fig. 9a is the same as that we used earlier (30, 33). Surface species are connected by reaction lines, while gas phase species that participate in these reactions or are generated as products are written next to these lines. The thickness of the reaction lines indicates relative rates of reactions, with dashed lines indicating the slowest reactions. Intersecting line segments separate the reaction lines into reactant and product sections. Arrows indicate allowable reaction directions. A single arrow indicates an irreversible reaction, while two arrows indicate reversible processes. Arrows positioned at equal distance from the intersecting lines indicate reactions at quasiequilibrium. Figure 9b shows how the various catalytic cycles are constructed from steps 1–33 in Fig. 1. (Note that the nonelementary step 8 does not appear in Fig. 9b.)

Catalytic cycles are composed of two or more reactions that determine the cycle rate and products formed. The

TABLE 8

Surface Coverages of Most Abundant Species at the Reactor Outlet for USY-S1, USY-S2, and USY-S3 at 773 K and ca. 15% Conversion

Species	USY-S1 125 kPa	USY-S2 131 kPa	USY-S3 123 kPa
H^+	9.4×10^{-1}	9.6×10^{-1}	9.7×10^{-1}
	1.4×10^{-5}	1.0×10^{-5}	6.5×10^{-6}
	4.9×10^{-2}	3.4×10^{-2}	2.5×10^{-2}
	1.4×10^{-6}	9.4×10^{-7}	6.9×10^{-7}
	7.8×10^{-3}	6.9×10^{-3}	4.6×10^{-3}
	1.6×10^{-3}	1.4×10^{-3}	9.2×10^{-4}
	7.6×10^{-5}	5.8×10^{-5}	4.3×10^{-5}

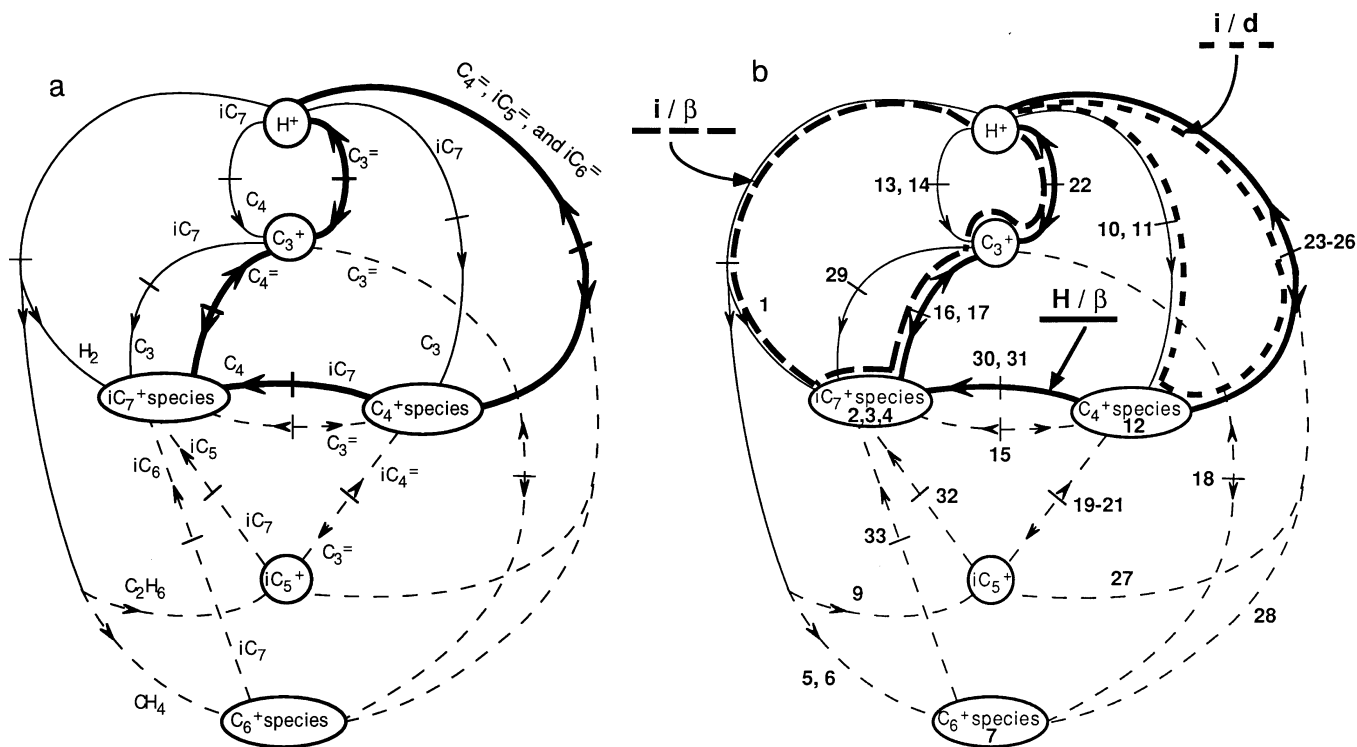


FIG. 9. Catalytic cycles for 2-methylhexane cracking (a) over USY-S1 at 773 K and 15% conversion at the reactor exit and (b) as composed of steps 1–33 in Fig. 1. Examples of initiation/ β -scission (i/β), initiation/desorption (i/d), and hydride ion transfer/ β -scission (H/β) cycles are also shown in (b).

three most important cycles for 2-methylhexane cracking are the initiation/ β -scission cycle (denoted as i/β), the initiation/desorption cycle (i/d), and the hydride ion transfer/ β -scission cycle (H/β). Examples of these three catalytic cycles are shown in Fig. 9b. Since some reactions can be part of more than one cycle, the reaction rates are not necessarily equal to the cycle rate of which they are a part. However, the steadystate approximation for surface species always holds; i.e., at a given condition and point in the reactor the concentration of surface intermediates is invariant.

Tables 6 and 7 list the forward and net rates of reactions that constitute the cycles presented here. Figure 10 shows how the rates of the important surface processes change with reactor length (or conversion) for USY-S1 and USY-S3. Initiation processes are composed of steps 1, 5, 6, 9, 10, 11, 13, and 14; desorption processes are the forward net rates of steps 22–28; β -scission processes are given by the forward net rates of steps 15–18, and 21; and hydride ion transfer processes are composed of steps 29–33. This figure and Table 9 show the decreases in turnover frequencies of all surface processes with increased steaming. This behavior explains the observed decrease in overall site time yields. As expected by the microcalorimetric data and model results, the differences between USY-S2 and USY-S3 are rather small (Table 9).

Carbenium Ion Initiation Cycles

One initiation cycle is the initiation/desorption cycle, such as the one that produces butene (see Fig. 9b). This cycle has a rate of $7 \times 10^{-3} s^{-1}$ for USY-S1 and $5 \times 10^{-4} s^{-1}$ for USY-S3 at a conversion ca. 15%. In such cycles, gas phase 2-methylhexane undergoes protolytic cracking, forming smaller paraffins and surface carbenium ions which can deprotonate and desorb as olefins. Because 2-methylhexane is sufficiently large, these cycles produce paraffins and olefins with three or more carbon atoms at 1 : 1 ratio.

TABLE 9

Effect of Catalyst Steaming on Reaction Rates

Reaction	Relative rates	
	USY-S2 (773 K, 131 kPa)	USY-S3 (773 K, 123 kPa)
Total initiation	0.37	0.36
Initiation to hydrocarbons	0.13	0.11
Hydride ion transfer	0.7–0.9 ^a	0.45–0.7 ^a
Oligomerization/ β -scission	0.75–1.2 ^a	0.5–1 ^a

Note. Rates are relative to USY-S1 at 773 K and 125 kPa. Conversion ca. 15%.

^aRelative rate change at the reactor entrance (conversion <0.5%).

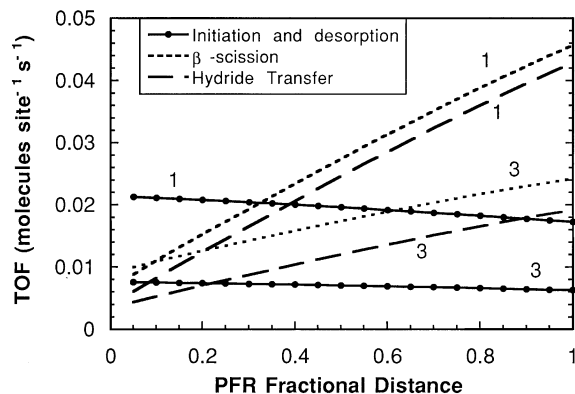


FIG. 10. Turnover frequencies of surface reactions with respect to reactor length for 2-methylhexane cracking over USY-S1 (1) and USY-S3 (3) at 773 K and 15% conversion.

The rate of the initiation/desorption cycles is determined by the initiation reactions, which, as in the case of isobutane cracking (30), are irreversible and relatively weak functions of conversion (Fig. 10). Although, the nature of these reactions (protolytic or other) is not fully understood, it appears that the rate of the initiation/desorption cycles decreases with steaming, which reduces the number and strength of the catalyst acid sites. The rates of initiation/desorption cycles for the more severely steamed USY-S3 are an order of magnitude lower than for USY-S1 (Tables 7 and 9). On USY-S1, these cycles contribute about 70% of the rate of all paraffin production at 0.5% conversion, and contribute about 25% at 15% conversion. On catalyst USY-S3, for similar conversions, these cycles contribute only 20% and 5%, respectively.

Another initiation cycle is the initiation/ β -scission cycle. These cycles include initiation reactions which yield hydrogen or methane, and the corresponding isoheptyl or hexyl cations which are large enough to undergo β -scission. Initiation/ β -scission cycles produce two olefins with three or more carbon atoms for each 2-methylhexane molecule they consume. One such cycle produces hydrogen, propylene, and butenes (see Fig. 9b). The rate of this cycle is $2 \times 10^{-3} \text{ s}^{-1}$ on USY-S1 and $4.5 \times 10^{-3} \text{ s}^{-1}$ on USY-S3 at ca. 15% conversion.

Initiation/ β -scission cycle rates are determined by the initiation reactions. Thus, like the initiation/desorption cycles, the rates of the initiation/ β -scission cycles are not affected by conversion and are expected to decrease with steaming severity which reduces catalyst acid strength. This behavior is observed for the cycle that produces methane. However, the rate of the hydrogen-producing cycle appears to increase slightly with steaming. This result cannot be explained directly by changes in acidity and is not in concert with our earlier finding for hydrogen production during isobutane cracking (30). The activation energy for hydrogen formation by initiation reactions dur-

ing 2-methylhexane cracking over USY-S1 is lower by ca. 6 kcal/mol than the value we reported for isobutane cracking (29). We speculate that this difference may be due to processes such as hydrogen production from coke or radical-like surface processes that are more important for the larger hydrocarbon and which we have not taken into account in the model. The rates of such processes have been reported to increase as the molecular weight of the reactant increases (44, 51). Others have explained a similar trend in the activation energies of protolytic reactions of 2-methylhexane and 2-methylpentane by invoking a compensation effect and temperature-induced changes in the number of active sites in the cracking of paraffins (16).

Hydride Ion Transfer Cycles

Hydride ion transfer/ β -scission cycles include a hydride ion transfer reaction from 2-methylhexane to a surface carbenium ion that results in a paraffin product and an isoheptyl cation on the surface. The latter cation undergoes β -scission producing C_3 or C_4 olefins and a smaller carbenium ion, which may deprotonate and desorb as an olefin or participate in other reactions. Thus, the hydride ion/ β -scission cycles yield both paraffins and olefins. If only paraffins and olefins with three or more carbon atoms are counted, these cycles produce equal amounts of paraffins and olefins. One example is the hydride ion/ β -scission cycle that produces butanes and propylene (see Fig. 9b): rates for the cycle are $3.6 \times 10^{-2} \text{ s}^{-1}$ on USY-S1 and $1.6 \times 10^{-2} \text{ s}^{-1}$ on USY-S3 at ca. 15% conversion. Other initiation and hydride ion transfer cycles that produce isopentane and isohexane play only a minor role overall.

The rates of hydride ion transfer/ β -scission cycles are determined by the rates of the hydride ion transfer reactions. These reactions, like initiation reactions, are irreversible. However, the rates of hydride ion transfer reactions are a strong function of carbenium ion coverage and therefore of conversion. When conversion increases, the carbenium ion coverages increase and the rates of hydride ion transfer processes increase accordingly (Fig. 10). For catalyst USY-S1, as conversion increases from about 0.5 to about 15%, the rates of these processes increase by a factor of 7. The decrease of acid strength caused by steaming reduces the coverages of surface carbenium ions and causes the rates of hydride ion transfer cycles to decrease. The rates of these cycles are reduced by as much as a factor of 2 from catalyst USY-S1 to USY-S3.

Figure 10 indicates that the rates of hydride ion transfer and β -scission reactions are significant even at low conversion. This behavior is caused by the presence of olefins produced by thermal radical cracking processes in the reactor preheating section above the catalyst. Carbenium ion coverages at the entrance of the reactor are a function not only of the acid strength of the catalyst, but also of the

partial pressure of the gas phase olefins produced by thermal cracking. We have incorporated measured values of these olefins in our model. For example, propylene and C_4 olefins from thermal cracking at the reaction conditions needed to achieve catalytic conversion of 15% are 0.022 and 0.031%, respectively, for USY-S1 and 0.065 and 0.089%, respectively, for USY-S3. The larger values are due to the larger reactor, with consequently larger volume, used to study USY-S3. This increase in the presence of gas phase olefins in the feed counters some of the effect of reduced acid strength, and therefore, at the reactor entrance the effect of steaming on the rates of hydride ion transfer processes is not as pronounced (Table 9). This result is in agreement with suggestions (52, 53) that catalytic cracking may also be initiated by protonation on Brønsted sites of olefins produced by thermal cracking of the reactants.

Product Distribution

The distribution of C_3 , C_4 , C_5 , and C_6 species depends on the relative rates of the catalytic cycles. As shown in Fig. 9b, catalytic cycles that dominate the cracking of 2-methylhexane are those that form C_3 and C_4 paraffins and olefins by hydride ion transfer, initiation, and β -scission reactions. Each of these cycles leads to the formation of one C_3 and C_4 species from each 2-methylhexane molecule consumed. Therefore, in agreement with experimental data (Fig. 5), the product stream consists mainly of C_3 and C_4 species at a ratio close to 1, and the distribution of C_3 , C_4 , C_5 , and C_6 species does not change appreciably with conversion or steaming. The oligomerization/ β -scission cycles and the initiation/ β -scission cycle that produces methane have only a small impact on selectivity, manifested as a small increase in the selectivity for C_3 species at the expense of C_4 species with reactor length. Although oligomerization/ β -scission cycles have a major impact on changes in the distribution of C_3 , C_4 , and C_5 species during isobutane cracking (30), they are not important for 2-methylhexane cracking.

During 2-methylhexane cracking, β -scission reactions follow initiation or hydride ion transfer reactions. The effects of conversion and steaming on the rates of these processes is a combination of the effects on the rates of initiation (hydrogen and methane producing steps only) and hydride ion transfer reactions. The rates of β -scission reactions increase as conversion and carbenium ion coverages increase (Fig. 10). Typically, for USY-S1, a rate increase by a factor of 5 accompanies a change in conversion from 0.5 to about 15%. Steaming reduces the rates of β -scission reactions by as much as a factor of 2. The increase with steaming of the rates of these processes at low conversion, shown in Table 9, is due to the increase in the rate of the hydrogen producing step. In agreement with our analysis of isobutane cracking (30), β -scission reactions are reversible processes.

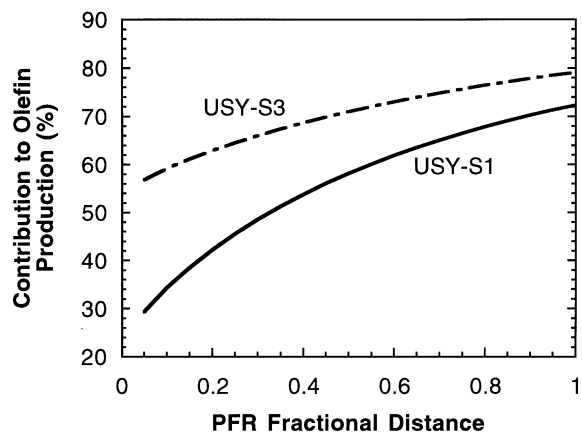


FIG. 11. Percentage contribution of β -scission cycles to the TOF of the total olefin production during 2-methyl hexane cracking on USY-S1 (—) and USY-S3 (---) catalysts at 773 K and 15% conversion.

The reversibility increases with conversion as the partial pressure of olefins in the gas phase increases, and in some cases the reverse rate can exceed the forward rate (step 18, Table 7).

Compared to the cracking of small paraffins like isobutane, β -scission reactions contribute significantly to the overall cracking chemistry of 2-methylhexane. For example, at about 10% conversion, the contribution of the initiation/ β -scission and the hydride ion transfer/ β -scission cycles to the TOF of olefin production is ca. 65% at the exit of the reactor for USY-S1, compared to a contribution of only ca. 15% for a similar catalyst in the case of isobutane cracking (30). Figure 11 shows the contribution of β -scission catalytic cycles to the TOF at 15% conversion for the formation of olefins over catalysts USY-S1 and USY-S3 with reactor length. This contribution is defined as 100 times the total rate of β -scission reactions divided by the sum of β -scission plus olefin desorption processes. This percentage is larger for the more severely steamed USY-S3, since its lower acid strength reduces the amount of olefins produced by the initiation/desorption cycle.

Bamwenda *et al.* (16) suggested that disproportionation reactions between surface carbenium ions and gas phase 2-methylhexane are important in paraffin production, while β -scission reactions are significant in the cracking of C_7 or larger olefins. They also concluded that propane, and C_6 and C_7 isomers are formed by hydride ion transfer, but C_4 and C_5 paraffins are formed exclusively by disproportionation reactions. We cannot explain why propyl, hexyl, and heptyl carbenium ions can abstract a hydride ion from 2-methylhexane, but butyl and pentyl carbenium ions cannot. The authors cite the cracking of C_6 molecules and n -nonane as cases where β -scission processes may not be important. We propose an alternate explanation, since β -scission reactions are not very important in the cracking of small hydrocarbons (30), and there are crucial differences

between the cracking of branched and normal paraffins (54, 55). For the latter, where a tertiary hydrogen is not present, initiation reactions tend to break the internal C-C bonds, leaving small carbenium ions on the surface. This behavior explains the limited role of β -scission reactions in C_6 and *n*-nonane cracking.

During analysis of isobutane cracking (30), we examined the possibility that a methide step, similar to the disproportionation reactions proposed by Bamwenda *et al.* (16), is important in the reaction chemistry. While our model was not able to provide a definitive answer, it suggested that such processes may be important only at very low conversions when the coverages of carbenium ions formed by oligomerization/ β -scission reactions are low. However, even in this case, hydride ion transfer processes became the dominant reactions as conversion increased and oligomerization/ β -scission reactions started producing the needed carbenium ions.

In the reaction scheme proposed by Bamwenda *et al.*, disproportionation reactions that include the transformation of C_7 and C_2 species to C_5 and C_4 or C_6 and C_3 species, C_7 and C_3 species to two C_5 species or C_6 and C_4 species, C_7 and C_4 to C_6 and C_5 species, as well as C_7 and C_5 to two C_6 species are important. The rates of these disproportionation reactions are expected to increase as the carbenium ion coverages increase with conversion. If such processes were indeed important, then at the wide range of conversions that we have studied we should observe significant changes with conversion in the distribution of the C_3 , C_4 , C_5 , and C_6 species in the product stream. Since we have not observed these changes (Fig. 5), we conclude that disproportionation reactions are not important in the cracking of 2-methylhexane over our catalysts. Such reactions do not need to be invoked to explain the products formed.

Paraffin/Olefin Ratio

As in our earlier work (30), we have defined the paraffin to olefin ratio as the ratio of paraffins versus olefins with three or more carbon atoms. These products result from initiation/desorption, initiation/ β -scission, and hydride ion transfer/ β -scission cycles, and therefore, the ratio is a function of the rates of these cycles (40). Note that a simple ratio of the rates of hydride ion transfer processes versus the rates of initiation reactions alone does not properly represent the paraffin to olefin ratio.

The initiation/desorption and the hydride ion transfer/ β -scission cycles produce paraffins and olefins with three or more carbon atoms at a ratio of 1 : 1. The initiation/ β -scission cycles produce two olefins with three or more carbon atoms. Since under our reaction conditions, these cycles dominate the reaction, our model explains the experimental data that show the paraffin to olefin ratio to be always lower than 1. This result agrees with that of Abbot and Wojciechowski (11).

The rates of the hydride ion transfer/ β -scission cycles increase with conversion. Figure 4 shows that the paraffin to olefin ratio changes only slightly with increasing conversion for USY-S1, while it changes significantly for USY-S2 and USY-S3. The changes in the paraffin to olefin ratio with conversion depend on which of the initiation cycles is dominant during the reaction. For catalyst USY-S1, about 80% of the activity due to initiation cycles is due to initiation/desorption cycles. Thus, the initial paraffin to olefin ratio for USY-S1 has a value close to 1. As conversion increases, the role of hydride ion transfer/ β -scission cycles increases, but this contributes paraffins and olefins at the same ratio of 1. Therefore, for USY-S1 the paraffin to olefin ratio increases only slightly with conversion as it approaches the limiting value of 1.

When the catalyst is steamed and its acid strength decreases, the rates of all surface reactions decrease. However, the initiation/desorption cycles are affected the most; steaming favors the initiation/ β -scission cycles. The model suggests that for USY-S2 and USY-S3 about 80% of the activity due to initiation cycles is due to the initiation/ β -scission cycles. Since these cycles produce only olefins, the initial value of the paraffin to olefin ratio decreases with steaming, and is considerably lower than 1 for USY-S2 and USY-S3 (Fig. 4). Subsequent contributions from the hydride ion transfer/ β -scission cycles, always at a paraffin to olefin ratio of 1, increase as conversion increases, and the value of the paraffin to olefin ratio increases toward its upper limit of unity. However, hydride ion transfer/ β -scission cycles cannot compensate for the changes in the relative rates of the various initiation cycles and the olefins produced by the initiation/ β -scission cycles. Thus, the paraffin to olefin ratio for the more severely steamed catalyst is always lower at the reactor exit.

CONCLUSIONS

We have developed a quantitative kinetic model for the cracking of 2-methylhexane and thus extended our initial studies of isobutane cracking (29, 30). As in the case of isobutane cracking, the model formulated for the larger hydrocarbon describes the experimentally observed changes in activity and selectivity with conversion and steaming severity very well.

The model results, in conjunction with ammonia microcalorimetry, show that the parameter ΔH_+ , the heat of stabilization of surface carbenium ions relative to surface protons, effectively represents surface acid strength, which determines catalyst activity and selectivity. As severity of steaming increases, the catalyst acid strength and consequently the rates of all surface reactions decrease. This decrease results in a lower observed overall site time yield and higher olefin selectivity for the more severely steamed catalyst.

The fundamental cracking chemistry of 2-methylhexane is the same as for isobutane cracking. For example, the rates of initiation cycles are weak functions of conversion, the rates of hydride ion transfer cycles increase with conversion, and the rates of all processes decrease with steaming. Olefin desorption reactions determine surface coverage of carbenium ions and, therefore, although these reactions are in quasi-equilibrium, they play a crucial role in influencing the rates of other surface processes.

The larger 2-methylhexane has more reaction pathways available to it than isobutane. Three catalytic cycles, the initiation/desorption cycle (paraffin/olefin = 1), initiation/ β -scission cycle (olefins only), and the hydride ion transfer/ β -scission cycle (paraffin/olefin = 1), dominate the cracking of 2-methylhexane, resulting in paraffin to olefin ratios less than or equal to 1. The paraffin to olefin ratio decreases with steaming mainly because of the effects of steaming on the relative rates of the various initiation cycles. Though oligomerization/ β -scission cycles are important for isobutane cracking, they are not important for 2-methylhexane cracking. However, β -scission reactions that follow initiation and hydride ion transfer reactions are an essential component of the chemistry of the larger hydrocarbon. In agreement with our analysis of isobutane cracking, we showed that, while some reactions may be more important than others at different stages of catalytic cracking, the concept of a rate determining step does not apply in catalytic cracking. The overall reaction rate is determined by a number of catalytic cycles, and the rates of these cycles are interdependent as several species and reactions are involved in more than one cycle.

ACKNOWLEDGMENTS

We sincerely appreciate the work done by the late Stan Koziol, who carried out all the kinetic measurements. We also thank Gale Hodge for the FTIR work and Drs. L. M. Aparicio and R. D. Cortright for contributions in model formulation and analysis. This work was partially supported by funds provided by Engelhard Corporation and the Office of Basic Energy Sciences of the U.S. Department of Energy (DE-FG02-84ER13183). This work was also supported in part by the U.S. Environmental Protection Agency and the Center for Clean Industrial and Treatment Technologies.

REFERENCES

1. McVicker, G. B., Kramer, G. M., and Ziemiak, J. J., *J. Catal.* **83**, 286 (1983).
2. Lombardo, E. A., and Hall, W. K., *J. Catal.* **112**, 565 (1988).
3. Lombardo, E. A., Pierantozzi, R., and Hall, W. K., *J. Catal.* **110**, 171 (1988).
4. Corma, A., Miguel, P. J., and Orchillés, A. V., *J. Catal.* **145**, 171 (1994).
5. Brenner, A., and Emmett, P. H., *J. Catal.* **75**, 410 (1982).
6. Haag, W. O., and Dessau, R. M., in "Proceedings, 8th International Congress on Catalysis, Berlin, 1984." Dechema, Frankfurt-am-Main, 1984.
7. Corma, A., Planelles, J., and Tomás, F., *J. Catal.* **94**, 445 (1985).
8. Abbot, J., and Wojciechowski, B. W., *Can. J. Chem. Eng.* **66**, 825 (1988).
9. Abbot, J., and Wojciechowski, B. W., *J. Catal.* **109**, 274 (1988).
10. Abbot, J., *J. Catal.* **126**, 628 (1990).
11. Abbot, J., and Wojciechowski, B. W., *J. Catal.* **107**, 451 (1987).
12. Mirodatos, C., and Barthomeuf, D., *J. Catal.* **114**, 121 (1988).
13. Shigeishi, R., Garforth, A., Harris, I., and Dwyer, J., *J. Catal.* **130**, 423 (1991).
14. Zhao, Y., Bamwenda, G. R., Groten, W. A., and Wojciechowski, B. W., *J. Catal.* **140**, 243 (1993).
15. Ono, Y., and Kanae, K., *J. Chem. Soc. Faraday Trans.* **87**(4), 663 (1991).
16. Bamwenda, G. R., Zhao, Y. X., and Wojciechowski, B. W., *J. Catal.* **148**, 595 (1994).
17. Blanding, F. H., *Ind. Eng. Chem.* **45**, 1186 (1953).
18. Weekman, V. W., and Nace, D. M., *AIChE J.* **16**, 397 (1970).
19. Allen, D. T., Marathe, P., and Harding, R., in "Computer-Aided Design of Catalysts" (E. R. Becker and C. J. Pereira, Eds.), p. 31. Dekker, New York, 1993.
20. Liguras, D. K., and Allen, D. T., *Ind. Eng. Chem. Res.* **28**(6), 665 (1989).
21. Liguras, D. K., and Allen, D. T., *Ind. Eng. Chem. Res.* **28**(6), 674 (1989).
22. Willems, P. A., and Froment, G. F., *Ind. Eng. Chem. Res.* **27**(11), 1966 (1988).
23. Willems, P. A., and Froment, G. F., *Ind. Eng. Chem. Res.* **27**(11), 1959 (1988).
24. Lox, E. S., and Froment, G. F., *Ind. Eng. Chem. Res.* **32**(1), 71 (1993).
25. Hillewaert, L. P., Dierickx, J. L., and Froment, G. F., *AIChE J.* **34**(1), 17 (1988).
26. Feng, W., Vynckier, E., and Froment, G. F., *Ind. Eng. Chem. Res.* **32**(12), 2997 (1993).
27. Baltanas, M. A., Raemdonck, K. K. V., Froment, G. F., and Mohedas, S. R., *Ind. Eng. Chem. Res.* **28**(7), 899 (1989).
28. Bamwenda, G. R., Zhao, Y. X., and Wojciechowski, B. W., *J. Catal.* **142**, 465 (1993).
29. Yaluris, G., Rekoske, J. E., Aparicio, L. M., Madon, R. J., and Dumesic, J. A., *J. Catal.* **153**, 54 (1995).
30. Yaluris, G., Rekoske, J. E., Aparicio, L. M., Madon, R. J., and Dumesic, J. A., *J. Catal.* **153**, 65 (1995).
31. Rekoske, J. E., Madon, R. J., Aparicio, L. M., and Dumesic, J. A., in "Proceedings, 10th International Congress on Catalysis, Budapest, 1992" (L. Guzzi, F. Solymosi, and P. Tetenyi, Eds.). Akadémiai Kiadó, Budapest, 1993.
32. Dumesic, J. A., Rudd, D. F., Aparicio, L. M., Rekoske, J. E., and Treviño, A. A., "The Microkinetics of Heterogeneous Catalysis." American Chemical Society, Washington, DC, 1993.
33. Yaluris, G., Madon, R. J., Rudd, D. F., and Dumesic, J. A., *Ind. Eng. Chem. Res.* **33**(12), 2913 (1994).
34. Haden, W. L., and Dzierzanowski, F. J., U.S. Patent 3,647,718 (1972).
35. Haden, W. L., and Dzierzanowski, F. J., U.S. Patent 3,506,594 (1970).
36. Brown, S. M., Durante, V. A., Reagen, W. J., and Speronello, B. K., U.S. Patent 4,493,902 (1985).
37. Sohn, J. R., DeCanio, S. J., Lunsford, J. H., and O'Donnell, D. J., *Zeolites* **6**, 225 (1986).
38. Chen, D., Sharma, S., Cardona-Martínez, N., Dumesic, J. A., Bell, V. A., Hodge, G. D., and Madon, R. J., *J. Catal.* **136**, 392 (1992).
39. Handy, B. E., Sharma, S. B., Spiewak, B. E., and Dumesic, J. A., *Meas. Sci. Technol.* **4**, 1350 (1993).
40. Yaluris, G., "Factors Controlling the Activity and Selectivity of Hydrocarbon Reactions on Acidic Catalysts." University of Wisconsin—Madison, 1995.
41. Dwyer, J., and Rawlence, D. J., *Catal. Today* **18**, 487 (1993).
42. Lechert, H., Meyer, A., Bezouhanova, C., Dimitrov, C., Nenova, V., and Taralanska, G., *J. Mol. Catal.* **35**, 349 (1986).

43. Wojciechowski, B. W., and Corma, A., "Catalytic Cracking: Catalysts, Chemistry, and Kinetics." Dekker, New York, 1986.
44. Gates, B. C., Katzer, J. R., and Schuit, G. C., "Chemistry of Catalytic Processes." McGraw-Hill, New York, 1979.
45. Corma, A., Faraldos, M., Mart'nez, A., and Mifsud, A., *J. Catal.* **122**, 230 (1990).
46. Corma, A., Faraldos, M., and Mifsud, A., *Appl. Catal.* **47**, 125 (1989).
47. Corma, A., and Orchillés, A. V., *J. Catal.* **115**, 551 (1989).
48. Wang, Q. L., Giannetto, G., and Guisnet, M., *J. Catal.* **130**, 471 (1991).
49. Wielers, A. F. H., Vaarkamp, M., and Post, M. F. M., *J. Catal.* **127**, 51 (1991).
50. Shertukde, P. V., Hall, W. K., Dereppe, J.-M., and Marcelin, G., *J. Catal.* **139**, 468 (1993).
51. Abbot, J., and Wojciechowski, B. W., *J. Catal.* **104**, 80 (1987).
52. Scherzer, J., *Catal. Rev.-Sci. Eng.* **31**(3), 215 (1989).
53. Stamires, D. N., and Turkevich, J., *J. Am. Chem. Soc.* **86**, 749 (1964).
54. Abbot, J., and Wojciechowski, B. W., *J. Catal.* **115**, 1 (1989).
55. Abbot, J., *Appl. Catal.* **47**, 33 (1989).